Supporting Information

Ultrathin Densified Carbon Nanotube Film with "Metal-like" Conductivity, Superior Mechanical Strength, and Ultrahigh Electromagnetic Interference Shielding Effectiveness

Yan-Jun Wan,[1,] Xiao-Yun Wang,[1] Xing-Miao Li,[1] Si-Yuan-Liao,[1] Zhi-Qiang Lin,[1] You-Gen Hu,[1] Tao Zhao,[1] Xiao-Liang Zeng,[1] Chun-Hong Li,[2] Shu-Hui Yu,[1] Peng-Li Zhu,[1,*] Rong Sun,[1] Ching-Ping Wong [3]*

[1] Shenzhen Institute of Advanced Electronic Materials, Shenzhen Institutes of Advanced Technology, Chinese Academy of Sciences, Shenzhen 518055, P.R. China;

[2] Fourth Phase Water Technologies, Wilmington, Delaware 19809, United States;

[3] School of Materials Science and Engineering, Georgia Institute of Technology, Atlanta 30332, United States.

*Corresponding Authors: yj.wan@siat.ac.cn (Y.-J. Wan); pl.zhu@siat.ac.cn (P-L. Zhu)

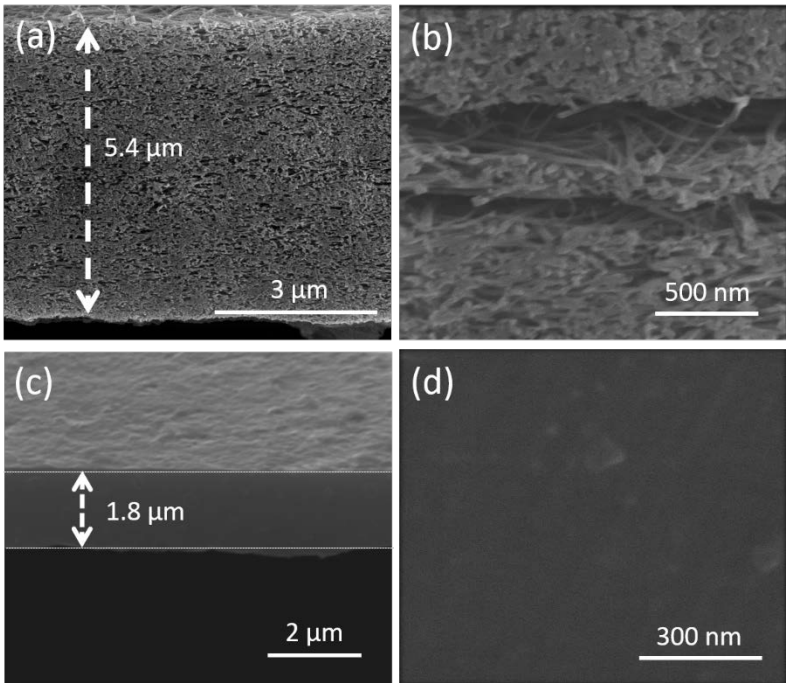

Figure S1 Thickness and microstructure changes of CNT film before and after densification process: SEM images of the cross-section of CNT film (a), (b) before and (c), (d) after densification. The thickness of CNT decreased significantly from ~ 5.4 µm to ~ 1.8 µm. Some pores could be observed and delamination occurred during the cutting process by focused ion beam, indicating weak tube-tube interaction before film densification.

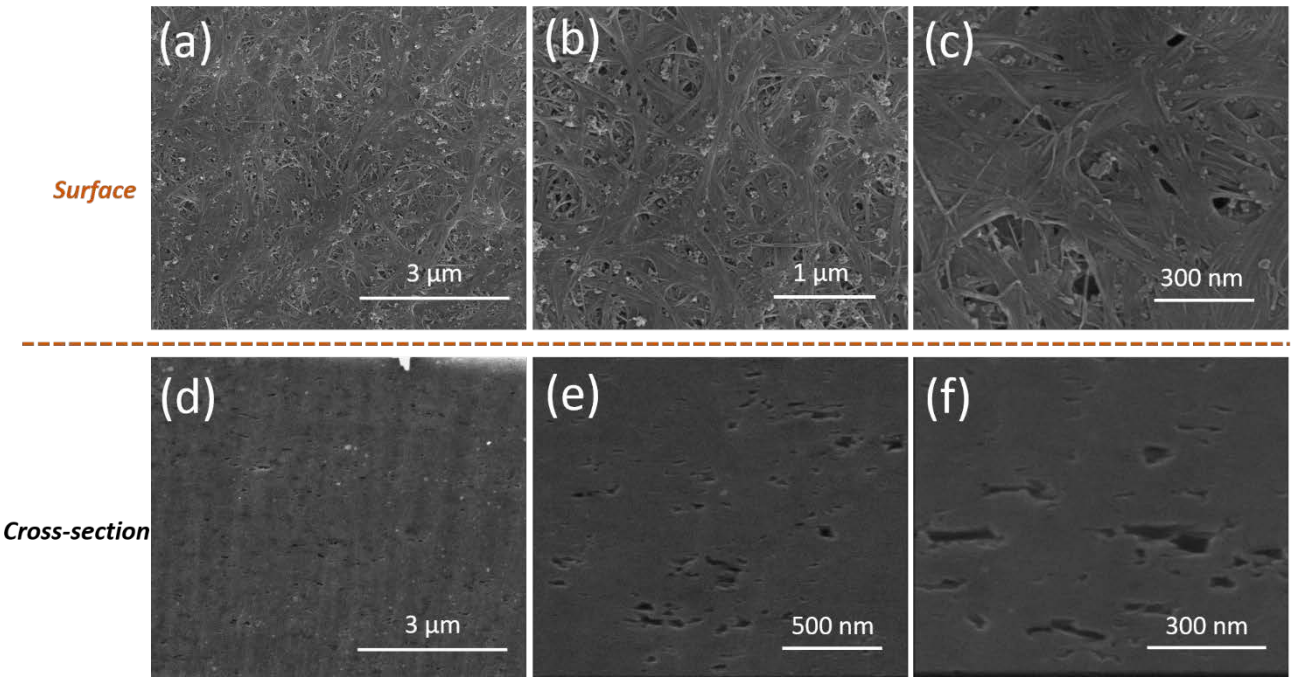

Figure S2 Morphology and structure of pristine CNT film after direct CSA treatment: (a), (b) and (c) SEM images of CNT film surface with different magnifications and (d), (e) and (f) SEM images of nanostructure in the cross-section of CNT film.

Mechanism of CNT densification

CNTs are composed of aromatic structures and each individual CNT can be viewed as a gigantic molecule. According to molecular orbital theory, one *2p* orbital from each carbon atom participates in the recombination of *2p* orbitals to form molecular π orbitals. Each molecular π orbital has a unique number of nodes. The higher the energy level, the more nodes the π orbital has. As electrons fill up the π orbitals, they will be in π orbitals with more and more nodes. The nodes can be interpreted as "+" or "-" in electron cloud distribution. In essence, electrons in higher energy π orbitals can be viewed as localizing more closely around some carbon atoms while staying away from other carbon atoms. The result is, even though a CNT molecule as a whole is charge neutral, there is partial positive charge around some carbon atoms while there is partial negative charge around the other carbon atoms across the CNT surface. This non-uniform electron density distribution (albeit very small) can explain the difference in ^{13}C NMR chemical shifts of aromatic molecules (e.g. pyrene).[1] Recent spectroscopic evidence also indicates non-uniform electron density distribution in CNT,[2] which can be interpreted as having strong dipoles or alternating positive and negative charges (or partial charges). Because of this charge separation, polar molecules such as water will preferentially interact with CNTs wound in CNT sheets to form an orderly layer of water,[3] behaving as a hydrophilic substance, even though there is no hydrophilic chemical functional group to interact with water molecules on a perfect CNT surface.

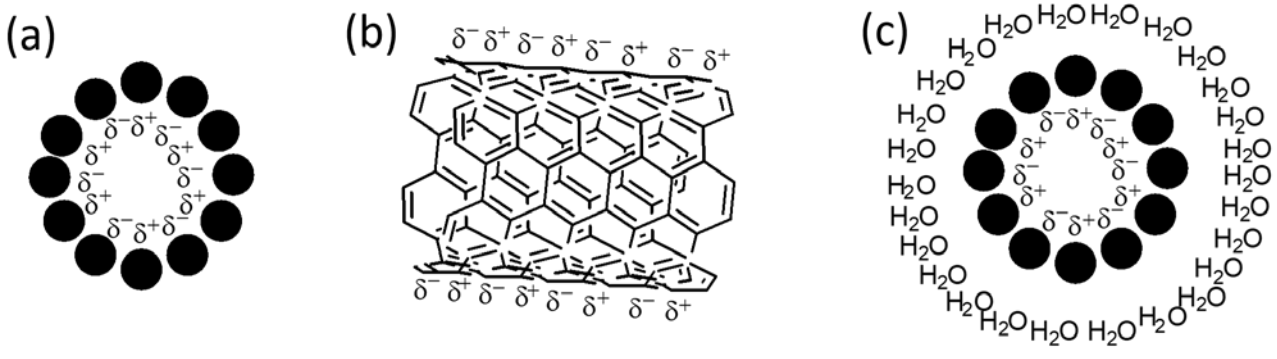

Figure S3 (a) Cross-sectional view of alternating positive and negative charges (or partial charges) across an individual CNT surface (only one molecular layer is shown for brevity); (b) Alternating charge distribution along a CNT surface; (c) Formation of a thin, orderly layer of water around individual CNT due to charge separation on CNT surface (only one molecular layer is shown for brevity).

Consistent with molecular orbital theory and spectroscopic evidence, greater charge separation corresponds to higher CNT hydrophilicity. One method to increase charge separation is to raise the energy level of π electrons in a CNT molecule. Because there are a very large number of π orbitals, the energy gap between highest occupied molecular orbital (HOMO) and lowest unoccupied molecular orbital (LUMO) is relatively small. Therefore, heat treatment of a CNT molecule can result in π electrons jumping from HOMO to LUMO. As the higher energy level LUMO has more nodes, more π electrons in the LUMO corresponds to greater charge separation in the CNT molecule. Experiments demonstrate that purified CNT sheets are highly hydrophilic after annealing under inert atmosphere. In such a purified CNT sheet, an adsorption layer of water forms around individual CNTs, establishing a nanometer gap between CNT surfaces and the water layer (**Figure S3** c). Air or water vapor could exist in this nanometer gap space. Treating purified CNT sheet with concentrated H_2SO_4 further stabilizes the adsorption of the water layer. It is envisioned that the water layer becomes more orderly due to the kosmotropic effect of SO_4^{2-}. The water layer becomes increasingly ordered as it nears the CNT surface. Adjacent CNTs join together through water layer surface minimization (**Figure S3** a). However, as air or water vapor occupies the nanometer gap, resistance likely arises as CNTs draw closer toward one another. Therefore, even though increased CNT alignment is visible under SEM after concentrated H_2SO_4 treatment and subsequent water rinse (Figure 2 c1-c4, in *Manuscript*), the densification is not sufficient to render a thin film with high tensile strength. The formation of orderly water layer wrapping around individual CNTs also prevents the infiltration of polar molecules such as water and H_2SO_4 into CNTs. Typical 2-5% weight loss in CNT thin film after concentrated H_2SO_4 treatment and subsequent water rinse suggests no significant water or H_2SO_4 infiltration.

$HClSO_3$ is highly hygroscopic and highly polar. When a CNT sheet is subsequently treated with $HClSO_3$, the orderly water layer is gradually thinned and becomes more polarized, which in turn relays the electrical field change to further enhance CNT charge separation. Such electrical field change further brings $HClSO_3$ molecules closer to CNT surface. Upon the removal of orderly water layer, infiltration of $HClSO_3$ molecules

into inner tube through tube end openings and defects occurs. Polar molecules in confined space could undergo phase transition to form chain-like structure.[4] The infiltration of highly polar $HClSO_3$ molecules further induces a substantial enhancement of charge separation in the CNTs. Consequently, attractive forces between adjacent CNTs increases dramatically. As excess $HClSO_3$ is slowly evaporated upon heating, individual CNTs are brought closer due to increased attractive force.

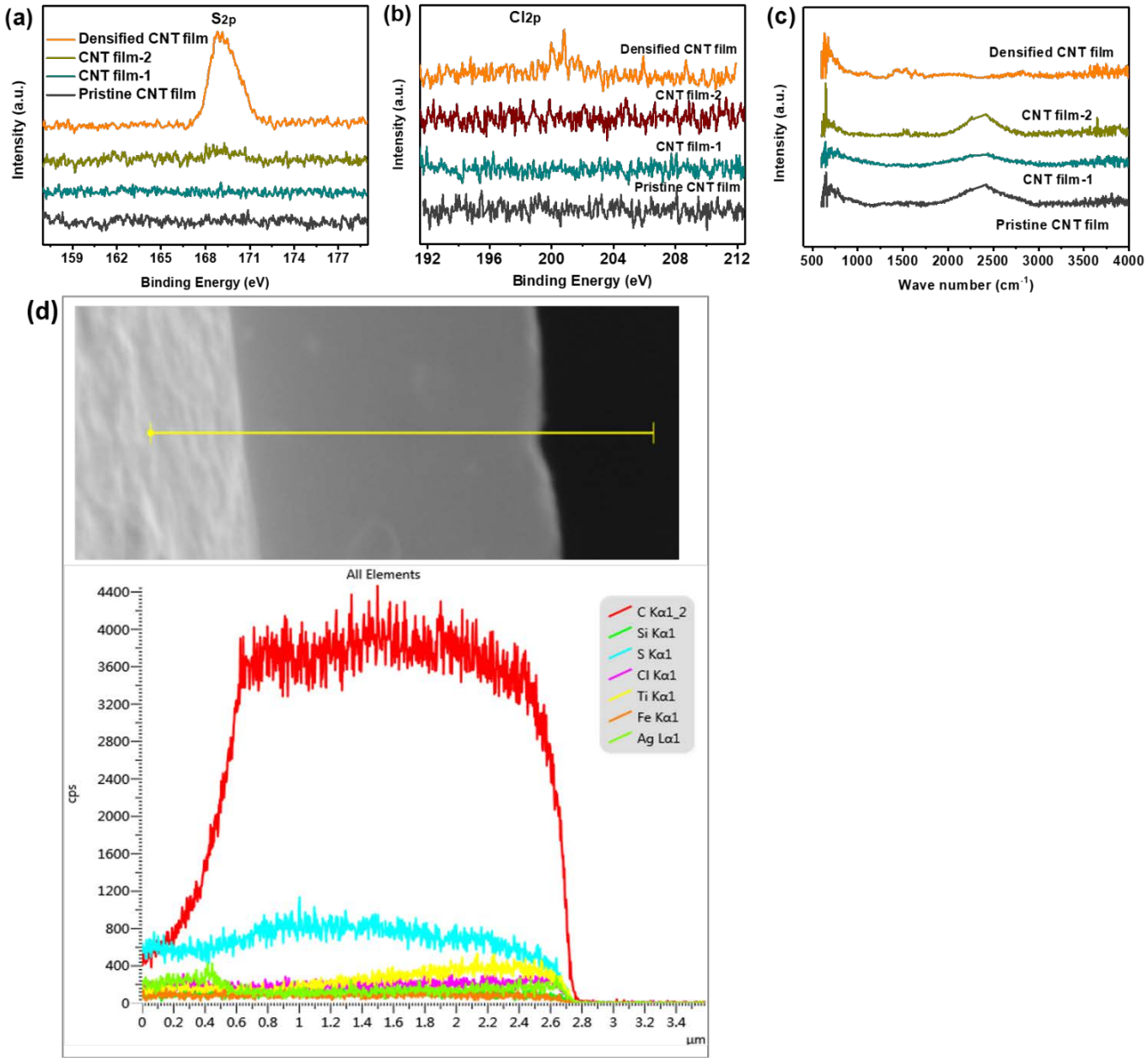

Figure S4 Chemical component characterizations of CNT films: (a) S2p spectra, (b) Cl2p spectra, (c) FT-IR spectra and (d) SEM image of cross-section of densified CNT film and the corresponding results of element line scanning. The weak intensity of signal line for S element combined with S2p XPS results suggest that there is infiltration of CSA molecules in CNT.

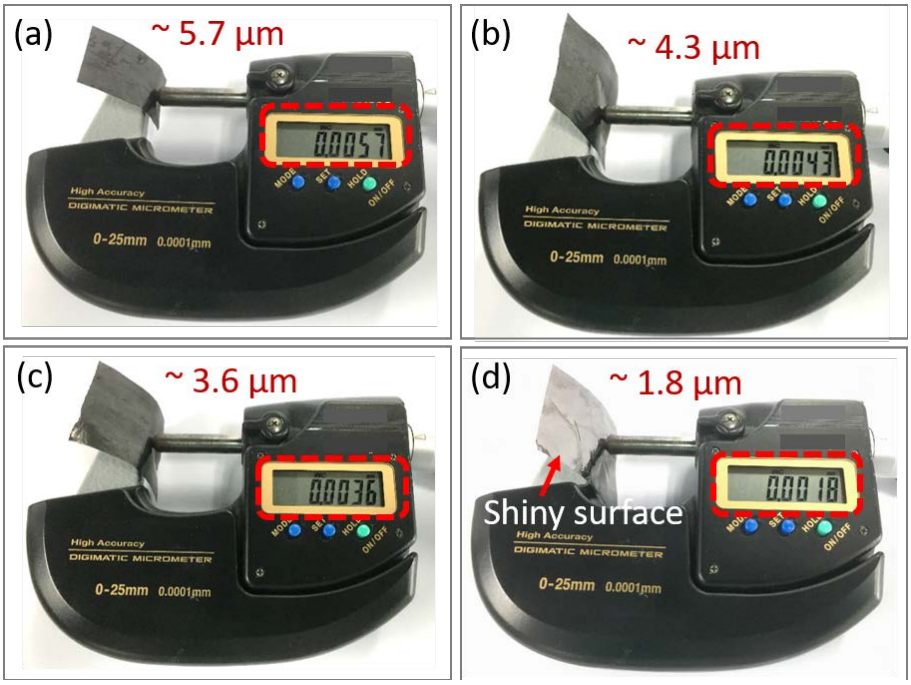

Figure S5 Thickness measurement of CNT films by micrometer with high accuracy of 0.0001 mm: (a) pristine CNT film with thickness of ~ 5.7 µm, consistent with the result of SEM images (~ 5.4 µm), (b) after thermal treatment (~ 4.3 µm), (c) after sulfuric acid treatment (~ 3.6 µm), and (d) after densification process (~ 1.8 µm), highly consistent with the result of SEM images (~ 1.8 µm). Note that the densified CNT film appears silvery due to the densification process.

Table S1 Physical properties of CNT films before and after treatment.

Sample	Pristine CNT film	CNT film-1	CNT film-2	Densified CNT film
Thickness (µm)	5.24	4.33	3.54	1.85
Aeral density (g/m^2)	2.89	2.23	2.10	2.58
Density (g/cm^3)	0.58	0.52	0.59	1.39
Conductivity (S/m)	68478	72198	127440	902712

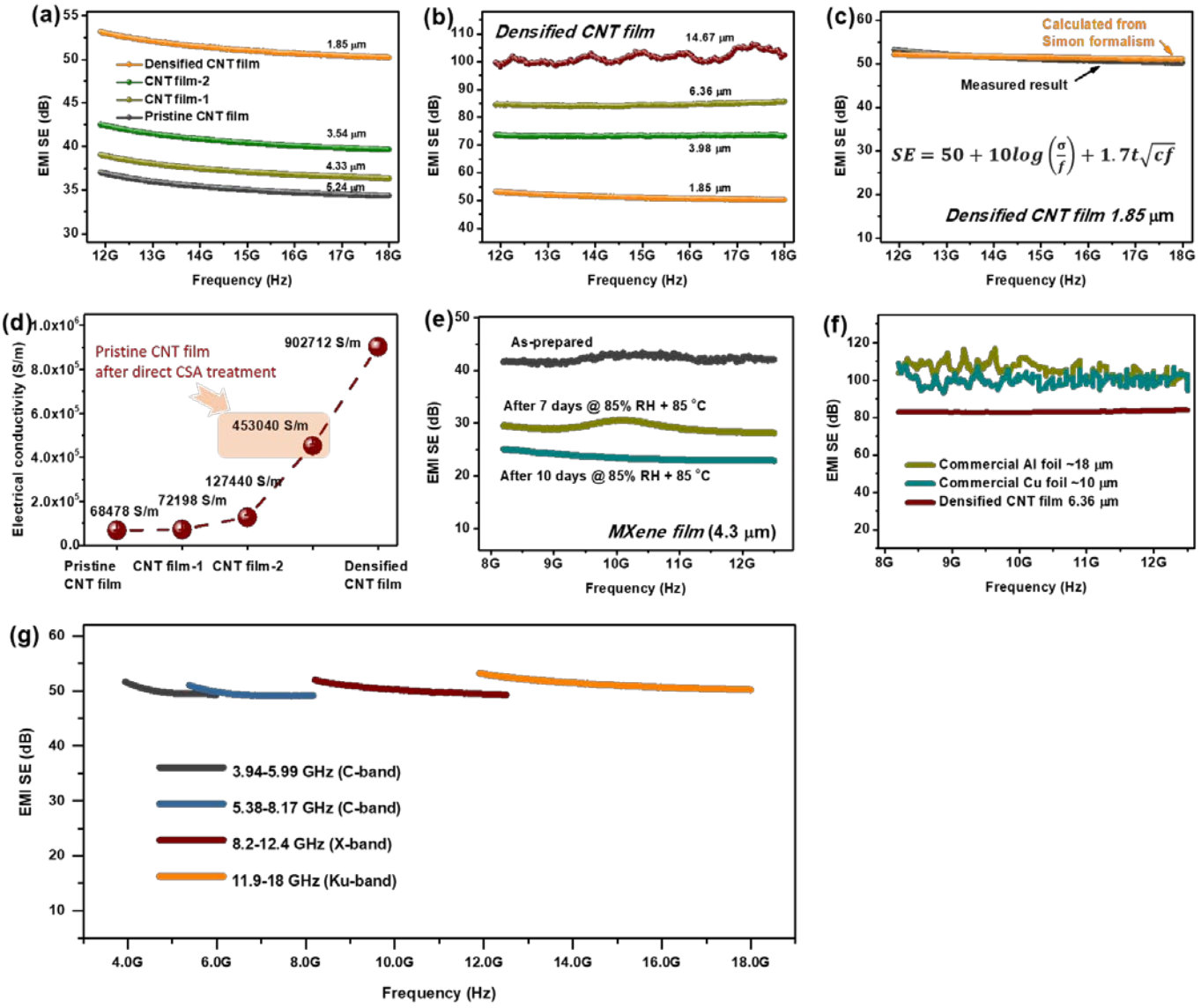

Figure S6 EMI shielding performance, electrical conductivity and reliability of shielding films. EMI SE of (a) CNT films with different treatment process and (b) densified CNT film with different thickness at Ku-band; (c) Comparison between theoretical EMI SE and experimental results of densified CNT film with thickness of 1.85 μm in Ku-band; (d) Electrical conductivity of CNT films; (e) SE of MXene film treated with 85 °C and 85% relative humidity; (f) SE Comparison between densified CNT film and commercial metal foil; (g) SE of densified CNT film with thickness of 1.85 μm in the broad frequency ranges of 4-18 GHz covering C-band, X-band and Ku-band. The discontinued SE curves should be ascribed to the waveguide holder with segmented frequency and the calibration error, which can also be found in reported literature.

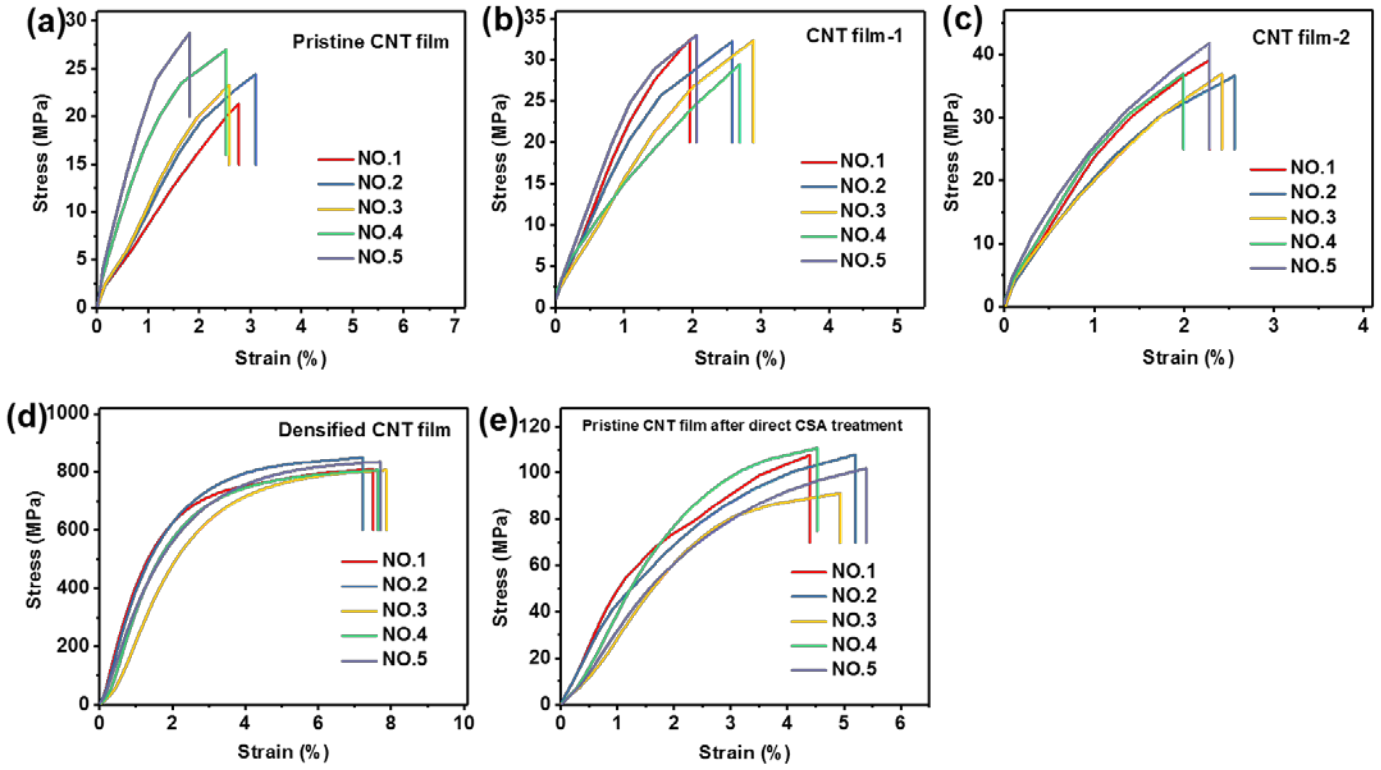

Figure S7 Stress-strain curves from tensile test of (a) pristine CNT film, (b) CNT film-1, (c) CNT film-2, (d) CNT film-3, (e) pristine CNT film after direct CSA treatment. Each sample has been measured with five sets of valid data.

Table S2 Summary of mechanical properties of CNT films

Sample	**Tensile strength** (MPa)	**Elongation at break** (%)	**Young's modulus** (GPa)	**Toughness**[#] (MJ m^{-3})
Pristine CNT film	24.9 ± 2.9	2.56 ± 0.48	1.37 ± 0.60	0.38 ± 0.06
CNT film-1	31.9 ± 1.4	2.43 ±0.51	1.75 ± 0.37	0.47 ± 0.07
CNT film-2	38.3 ± 2.2	2.31 ± 0.21	2.24 ± 0.19	0.54 ± 0.05
Densified CNT film	822.5 ± 21.0	7.59 ± 0.27	36.94 ± 6.59	48.43 ± 1.08
Pristine CNT film after direct CSA treatment	103.9 ± 7.8	4.8 ± 0.43	3.99 ± 0.89	3.33 ± 0.32

[#] Calculated by integrating stress-strain curves.

Equation part

(1) The reflection loss (SE_R) an be evaluated by the Fresnel's equation for a highly conductive shield as follows:

$$SE_R(dB) = 20\log\frac{(\eta+\eta_0)^2}{4\eta\eta_0} = 39.5 + 10\log\frac{\sigma}{2\pi f\mu} \qquad (1)$$

Absorption loss (SE_A) for non-magnetic and conducting shielding materials can be expressed as follows:

$$SE_A = 20\log e^{\alpha d} = 20\left(\frac{d}{\delta}\right)\log e = 8.68\left(\frac{d}{\delta}\right) = 8.68d\sqrt{\pi f\mu\sigma} \qquad (2)$$

$$\alpha = \omega\sqrt{\frac{\mu\varepsilon}{2}\left[\sqrt{1+\left(\frac{\sigma}{\omega\varepsilon}\right)^2}-1\right]} \qquad (3)$$

where η and η_0 are the impedances of the shield and air, respectively, σ and μ are the electrical conductivity and the magnetic permeability of the shield, respectively, f is the frequency of the incident electromagnetic waves, and ω is angular frequency and ε is dielectric permittivity.

(2) The EMI SE was calculated from the scattering parameters (S_{11} and S_{21}) by the following formulas:

$$R = |S_{11}|^2 \qquad (4)$$

$$T = |S_{21}|^2 \qquad (5)$$

$$A + R + T = 1 \qquad (6)$$

$$SE_{Total}(dB) = -10\,log(P_{out}/P_{in}) = -10\,log\,T \qquad (7)$$

$$SE_R(dB) = -10\,log(1-R) \qquad (8)$$

$$SE_A(dB) = SE_{total} - SE_{ref} \qquad (9)$$

Where R, T and A are the reflection, transmission and absorption coefficients, respectively. P_{in} and P_{out} are the incident and transmitted power, respectively. SE_{Total}, SE_R and SE_A are the total, reflective and absorptive EMI SE, respectively.

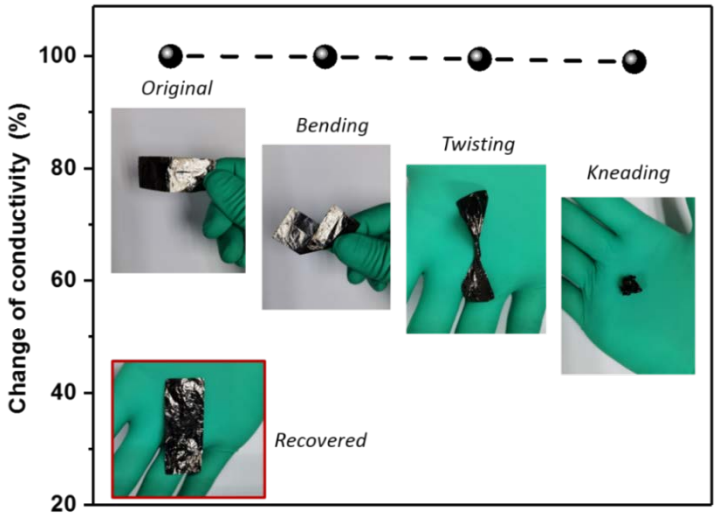

Figure S8 Electrical conductivity changes of densified CNT film after bending, twisting and kneading.

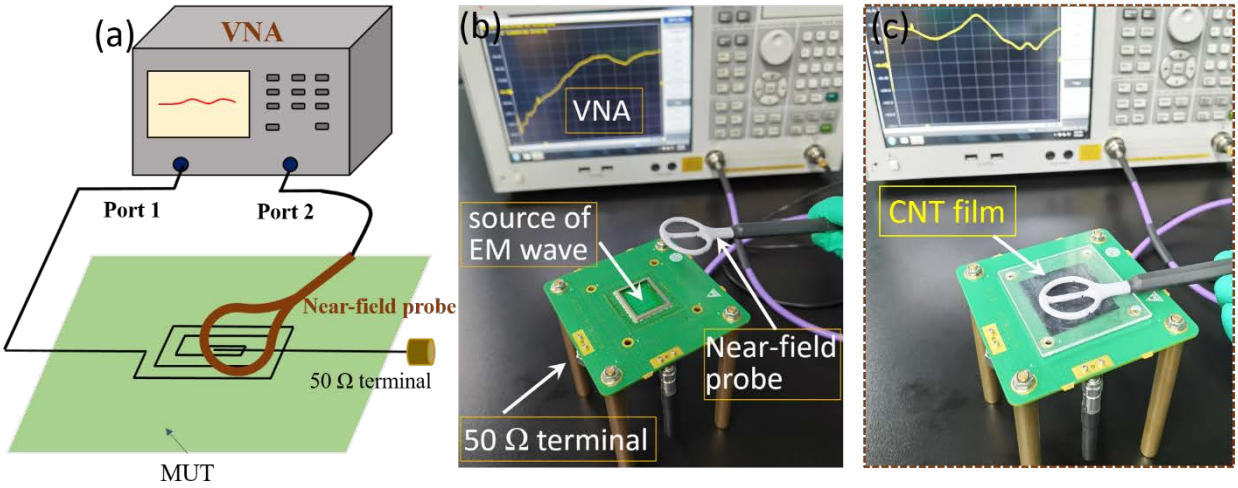

Figure S9 (a) Schematic and photograph of measurement setup for near-field shielding effectiveness (b) without and (c) with shielding film.

We used a test board embedded loop-antenna as the source of electromagnetic wave, and near-field probe (H-field, XF-R 400-1, Langer EMV-Technik) with high resolution combined with vector network analyzer (VNA, Keysight, E5071C) was employed to measure the near field radiation, as shown in Figure S8. The near-field shielding effectiveness is then calculated by taking the ratio of insertion loss difference (S_{21}) with and without CNT film, as shown in Figure 4g. The radiation isolation of near field has a significant improvement with the CNT film, The near-field shielding performance of densified CNT film is 20-40 dB in the frequency range of 0.5 GHz to 6 GHz with only 1.85 μm and the SE for high frequency is relative higher due to skin depth decreasing.

Table S3 Comprehensive performance of various shielding materials.

Sample	SE_{Total}	SE_A	SE_R	A	R	Ref.
Cu-wrapped nanofiber membranes	54.1	44.5	9.6	--	--	*Adv. Mater. 2020, 1908496*
Ag-wrapped nanofiber membranes	55.1	40.4	14.7	--	--	
Annealed Ti_3CNT_x film	116	98	18	--	--	*Science, 2020, 369, 446-450.*
MXene film (*Filtration*)	58	35.3	22.7	--	--	*Science 2016, 353, 1137-1140*
CPAN NF/ CPAN NF/Ag NP membrane	83	63	20	--	--	*NPG Asia Materials, 2018, 10(8): 749-760.*
CPAN NF/Cu NP membrane	56	38.5	17.5	--	--	
CPAN NF/Ni NP membrane	54	39	15	--	--	
Pristine MXene film	60	41	19	--	--	*Adv. Funct. Mater. 2019, 1906996*
	67.5	49	18.5	--	--	
MXene film (*Blade coating*)	46.1	32.6	13.5	--	--	*Adv. Mater. 2020, 2001093*
Crumpling MXene coating	46	26.3	19.7	--	--	*Adv. Funct. Mater. 2019, 1907451*
	52	32	20	--	--	
MXene/CNF paper	25	19	6	--	--	*ACS Nano 2018, 12, 4583-4593*
	26	20.5	5.5	--	--	
Alternating MXene/CNF	38	19.6	18.4	0.015	0.984	*ACS Appl. Mater. Interfaces 2020, 12, 4895-4905*
	39.6	21.5	18.1	0.016	0.983	
AgNW/CNF	82	61.5	20.5	--	--	*ACS Appl. Mater. Interfaces 2020, 12, 18023-18031*
	101	74	27	--	--	
MXene/ANF film	24.5	18.5	6	0.232	0.767	*ACS Appl. Mater. Interfaces 2020, 12, 26485-26495*
MXene/PEDOT:PSS	28.2	15.7	12.5	--	--	*ACS Appl. Mater. Interfaces 2018, 10, 44787-44795*
	42.1	27.5	14.6	--	--	
Graphene film	38.1	23.1	15	0.0347	0.9651	*Adv. Mater. 2020, 1907411*
	44.5	27.3	17.2	0.0174	0.9825	
CNT/Graphene film	80	64	16	--	--	*Carbon 162 (2020) 490-496*
CNT/WPU film	61.5	45.4	16.1	--	--	*Carbon, 2016, 96: 768-777*
	49	31	18			
Fe_3O_4/graphene	24	16	8	--	--	*J. Mater. Chem. A, 2015, 3, 2097-2107*
PPy/PDA/AgNW	25.9	17	8.9	--	--	*Nanoscale, 2017, 9(46): 18318-18325.*
	48	32	16	--	--	

Table S4 Comprehensive performance of various shielding materials.

Sample	SE	Thickness (μm)	Density (g/cm^3)	Conductivity (S/m)	Tensile strength (MPa)	Reliability (acid/alkali, 85% RH+85 °C)	Ref.
Densified CNT film	51.2	1.85	1.39	9.027- E5	822 ± 21	Yes	***This work***
	73.3	3.98					
	84.5	6.36					
	101.4	14.67					
Cu-wrapped nanofiber membranes	53.2	2.5	1.6	7.66-E5	35	No	***Adv. Mater. 2020, 1908496***
Ag-wrapped nanofiber membranes	55.1	2.5	1.97	3.12-E6	--	No	
Annealed Ti_3CNT_x film	75.1	10	--	2.475-E5	--	No	***Science, 2020, 369, 446-450.***
	83.0	20	--		--	No	
	97.1	30	--		--	No	
	116.2	40	--		--	No	
MXene film (*Filtration*)	68	11	2.39	4.665-E5	--	No	***Science 2016, 353, 1137-1140***
Al foil	66	8	2.71	2.8-E7		No	
Cu foil	70	10	8.96	8.0-E7		No	
Cu/graphene film	52	9	2.1	5.88-E6	--	No	***Small 2018, 14, 1704332***
CPAN NF/metal membrane	85.2	35	2.37	5.6-E6	27	No	***NPG Asia Materials, 2018, 10(8): 749-760.***
Pristine MXene film	54	2.5	3.9	1.04-E6	102 ± 11	No	***Adv. Funct. Mater. 2019, 1906996***
MXene film (*Blade coating*)	53.5	2.4	4.3	1.02-E6	480 ± 35	No	***Adv. Mater. 2020, 2001093***
Crumpling MXene coating	52	10	-	2.9-E5	-	No	***Adv. Funct. Mater. 2019, 1907451***
MXene/CNF paper	25	16.7	1.13	10	135 ± 7	No	***ACS Nano 2018, 12, 4583-4593***
	26	7.4	1.62	116	44 ± 5	No	
FC-ANF/CNT	41.9	568	0.0403	230	5	Yes	***ACS Nano 2020, 14, 688-697***
	35.6	396	0.0403	230	5		
CNT/PTA film	30	1	--	2.04-E5	1250 ± 119 (Orientation) / 205 (Perpendicular)	Yes	***Carbon 2020, 158, 472-480***
Alternating MXene/CNF	39.6	35	1.61	100	115	No	***ACS Appl. Mater. Interfaces 2020, 12, 4895-4905***
AgNW/CNF	101	44.5	--	5.57-E5	60.7	No	***ACS Appl. Mater. Interfaces 2020, 12, 18023-18031***

MXene/ANF film	34.6	21.4	2	1-E4	300 ± 10	No	*ACS Appl. Mater. Interfaces 2020, 12, 26485-26495*
MXene/PEDOT:PSS	42.1	11.1	1.94	3.4-E4	13.7	No	*ACS Appl. Mater. Interfaces 2018, 10, 44787-44795*
LBL MXene-CNT	3	0.207	2.84	1.3-E4	25	No	*Adv. Funct. Mater. 2018, 28, 1803360*
Al ion-reinforced MXene film	80	39	--	2.65-E5	83.2	No	*J. Mater. Chem. C, 2020, 8, 1673-1678*
Graphene film	38.1	4	1.49	1.34-E5	145	Yes	*Adv. Mater. 2020, 1907411*
	44.5	8	1.49	1.34-E5		Yes	
Graphite film	27.8	0.385	2.25	2.6-E5	110	Yes	*ACS Nano, 2020, 14(3): 3121-3128.*
8% Graphene-epoxy composites	40	> 100	1.4	2.9-E4	540	Yes	*Nat. Commun., 2020, 11(1): 1-10.*
CNT/Graphene film	80	50	-	-	1.8	Yes	*Carbon 162 (2020) 490-496*
CNT/WPU film	61.5	50	1.2	2.1-E3	2.6	Yes	*Carbon, 2016, 96: 768-777*
Fe_3O_4/graphene	24	200	0.78	5-E3	--	NO	*J. Mater. Chem. A, 2015, 3, 2097-2107*
PPy/PDA/AgNW	10	84.7	0.277	0.03	--	No	*Nanoscale, 2017, 9(46): 18318-18325.*
	25.9	95.1	0.278	55			
PEI/graphene	21	2300	0.31	3.9-E(-8)	8.5	Yes	*ACS Appl. Mater. Interfaces 2013, 5, 2677-2684*
RGO-CNT	57.6	15	1.45	2.74-E5	--	Yes	*Carbon 2018, 133,316*

NOTES: CNT: carbon nanotube; LBL: layer by layer; CPAN NF: polyacrylonitrile nanofiber; CNF: cellulose nanofiber; ANF: aramid nanofiber; FC: fluorocarbon; PTA: polytriazole; WPU: water-borne polyurethane; PEDOT:PSS: Poly(3,4-ethylenedioxythiophene)-poly(styrenesulfonate); PPy: polypyrrole; PDA: polydopamine; AgNW: silver nanowire.

References

1. Hernández-Trujillo, J.; García-Cruz, I.; Martínez-Magadán, J. M. J. C. p., Topological Analysis of the Electron Density and of the Electron Localization Function of Pyrene and Its Radicals. *Chem. Phys.* **2005**, *308*, 181-192.

2. Lin, H.; Lagoute, J.; Repain, V.; Chacon, C.; Girard, Y.; Ducastelle, F.; Amara, H.; Loiseau, A.; Hermet, P.; Henrard, L. J. P. R. B., Imaging the Symmetry Breaking of Molecular Orbitals in Single-Wall Carbon Nanotubes. *Phys. Rev. B* **2010**, *81*, 235412.

3. Homma, Y.; Chiashi, S.; Yamamoto, T.; Kono, K.; Matsumoto, D.; Shitaba, J.; Sato, S. J. P. r. l.,

Photoluminescence Measurements and Molecular Dynamics Simulations of Water Adsorption on the Hydrophobic Surface of a Carbon Nanotube in Water Vapor. *Phys. Rev. Lett.* **2013**, *110*, 157402.

4. Ma, X.; Cambré, S.; Wenseleers, W.; Doorn, S. K.; Htoon, H. J. P. r. l., Quasiphase Transition in a Single File of Water Molecules Encapsulated in (6, 5) Carbon Nanotubes Observed by Temperature-Dependent Photoluminescence Spectroscopy. *Phys. Rev. Lett.* **2017**, *118*, 027402.